Molecular Cell, Volume *63*

Supplemental Information

Cryo-EM of Mitotic Checkpoint Complex-Bound APC/C Reveals Reciprocal and Conformational Regulation of Ubiquitin Ligation

Masaya Yamaguchi, Ryan VanderLinden, Florian Weissmann, Renping Qiao, Prakash Dube, Nicholas G. Brown, David Haselbach, Wei Zhang, Sachdev S. Sidhu, Jan-Michael Peters, Holger Stark, and Brenda A. Schulman

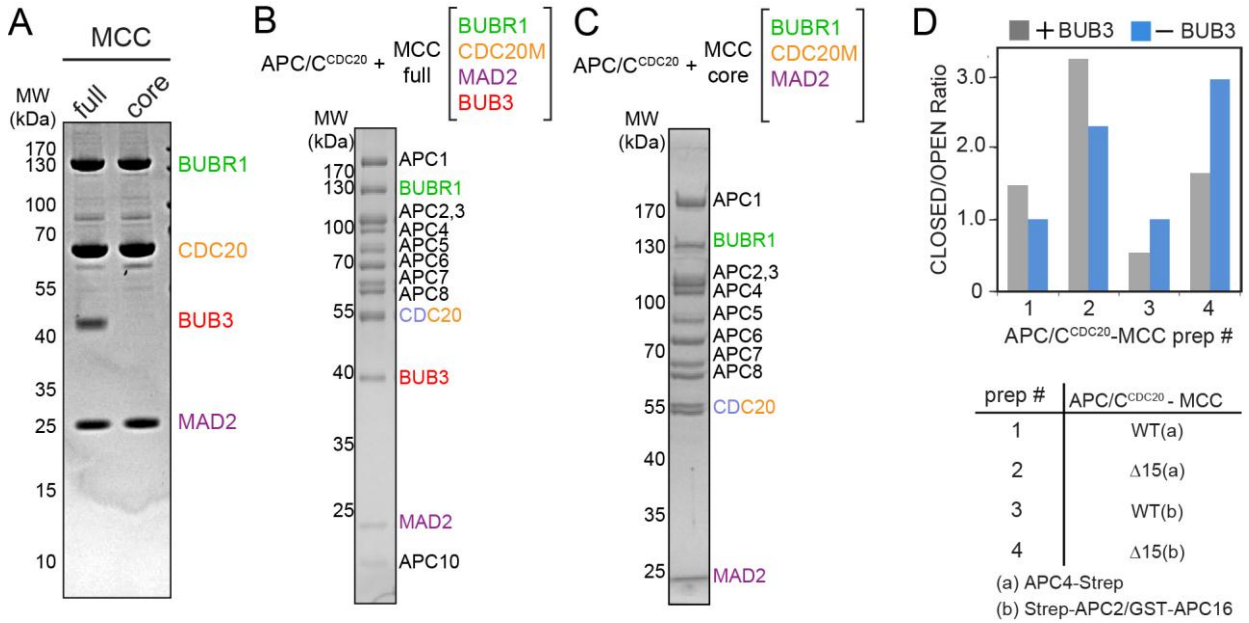

Figure S1. Common features of APC/C^{CDC20} complexes with MCC and the evolutionarily conserved MCC core (CDC20–MAD2–BUBR1) that lacks BUB3. Related to Figure 1.

(A-C) SDS-PAGE analysis of purified full MCC or the evolutionarily conserved core that lacks BUB3, alone or in complexes with APC/C^{CDC20}.
(D) To determine whether APC/C^{CDC20}–MCC core maintains the general conformational properties of APC/C^{CDC20}–MCC, or whether BUB3 plays a role, four matched pairs of APC/C^{CDC20} complexes with full or core MCC, with or without APC15 were prepared, analyzed by single particle negative stain EM, and 3D reconstructions were calculated. As described in Table S2, we tested two distinct affinity tag purification schemes (either APC4-Twin-Strep or double-affinity Twin-Strep-APC2/GST-APC16). The bar graph shows ratio of particles in 3D classes with CDC20$_A$–MCC in CLOSED over OPEN conformations. Excluding BUB3 had no consistent effect on the increased formation of CLOSED configurations in the absence of APC15.

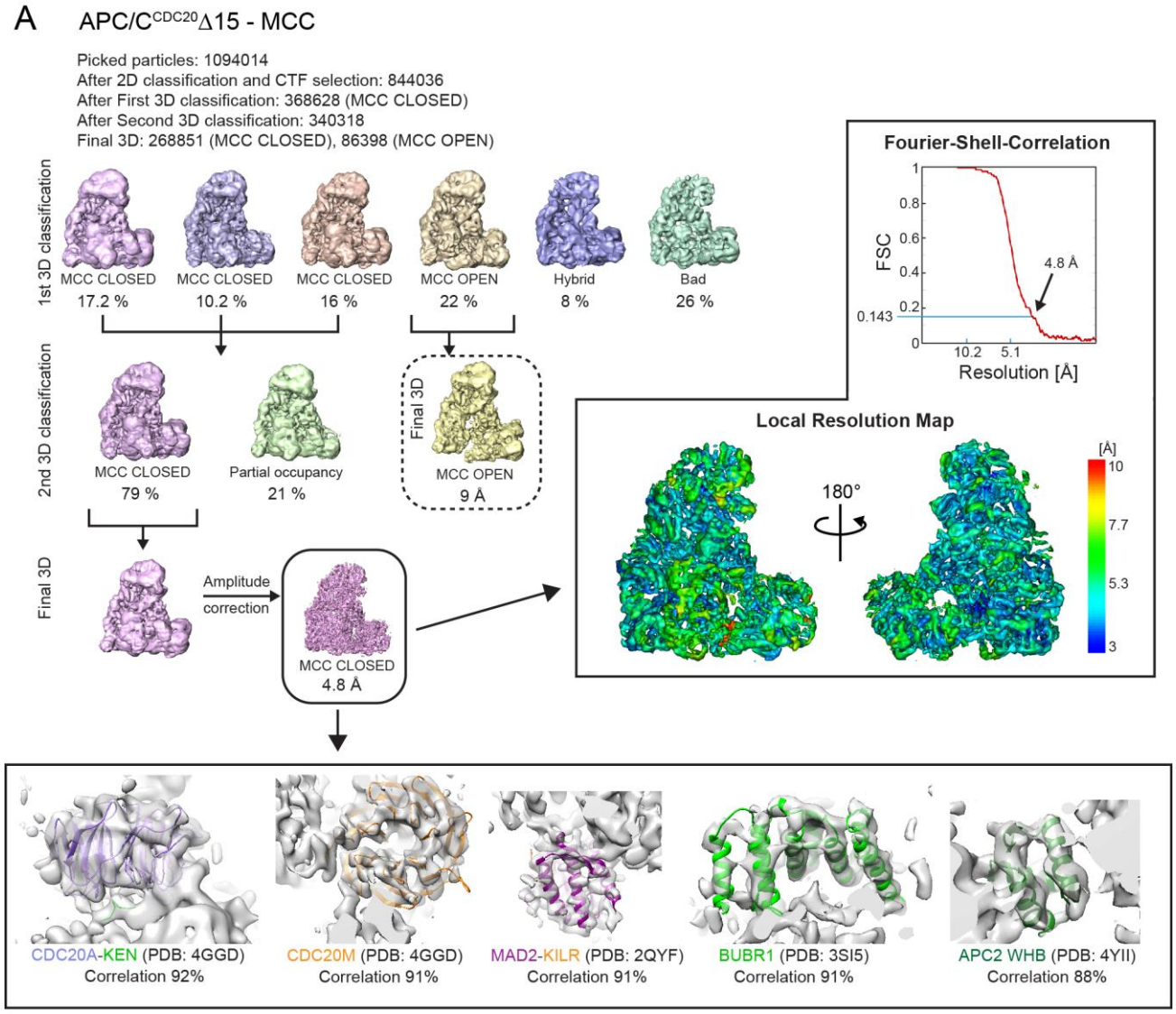
A
APC/C^CDC20Δ15 - MCC
Picked particles: 1094014
After 2D classification and CTF selection: 844036
After First 3D classification: 368628 (MCC CLOSED)
After Second 3D classification: 340318
Final 3D: 268851 (MCC CLOSED), 86398 (MCC OPEN)
1st 3D classification
MCC CLOSED 17.2 %
MCC CLOSED 10.2 %
MCC CLOSED 16 %
MCC OPEN 22 %
Hybrid 8 %
Bad 26 %
2nd 3D classification
MCC CLOSED 79 %
Partial occupancy 21 %
Final 3D
MCC OPEN 9 Å
Final 3D
Amplitude correction
MCC CLOSED 4.8 Å
Fourier-Shell-Correlation
FSC
4.8 Å
0.143
Resolution [Å]
Local Resolution Map
180°
[Å]
10
7.7
5.3
3
CDC20A-KEN (PDB: 4GGD) Correlation 92%
CDC20M (PDB: 4GGD) Correlation 91%
MAD2-KILR (PDB: 2QYF) Correlation 91%
BUBR1 (PDB: 3SI5) Correlation 91%
APC2 WHB (PDB: 4YII) Correlation 88%

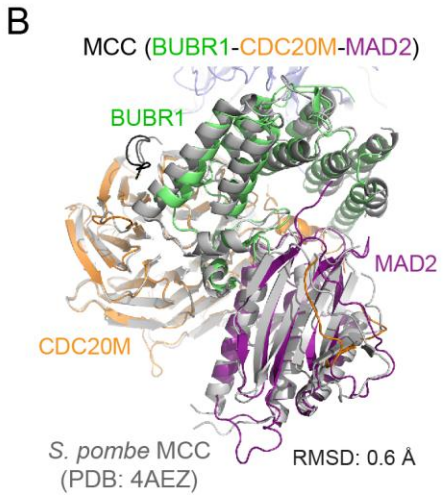
B
MCC (BUBR1-CDC20M-MAD2)
BUBR1
MAD2
CDC20M
S. pombe MCC (PDB: 4AEZ)
RMSD: 0.6 Å

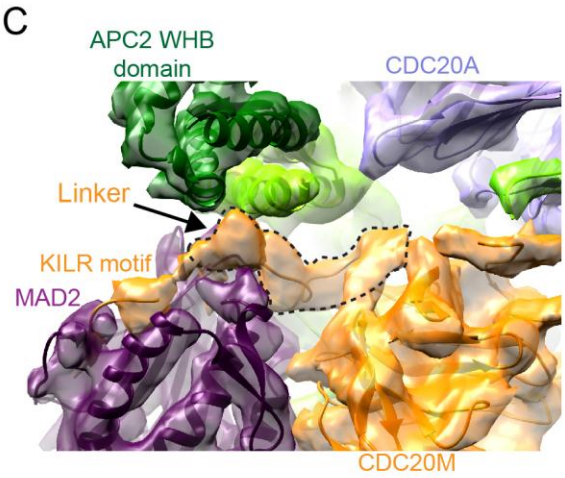
C
APC2 WHB domain
CDC20A
Linker
KILR motif
MAD2
CDC20M

Figure S2. Cryo EM reconstruction of APC/C^{CDC20}-MCC. Related to Figure 2.

(A) To obtain a cryo EM reconstruction for APC/C^{CDC20}Δ15-MCCcore, an initial 1,142,501 particle images were collected of which 67% were kept after 2D classification and particle sorting according to CTF parameters. After the first 3D classification, 42.4% of the particles divided in 3 subclasses displayed the CLOSED conformation for APC/C^{CDC20}Δ15-MCC, 1 class comprising 22% of the particles was OPEN, and the remaining 34% were classified as hybrid or bad. The 86,398 particles corresponding to APC/C^{CDC20}Δ15-MCC in the OPEN configuration were used to determine a final 3D structure to 9 Å, whereas those particles classified as corresponding to the CLOSED configuration were subjected to a second round of 3D classification. Ultimately, 268,851 particles in a subclass with full MCC occupancy were used for the final refinement to obtain a 3D structure at 4.8 Å resolution. The Gold-standard Fourier-Shell-Correlation ($FSC_{0.143}$) was used to determine the final overall resolution and we show opposing views of local resolution maps to demonstrate the resolution range. Crystal structures of human CDC20, BUBR1, and MAD2 were individually docked in the map using Chimera (Bolanos-Garcia et al., 2011; Tian et al., 2012; Yang et al., 2007), with additional elements generated by homology modeling and manual building in COOT (Emsley and Cowtan, 2004). A model for the human MCC core bound to APC/C^{CDC20}Δ15 was initially generated in Chimera (Pettersen et al., 2004), by fitting the high resolution structures of APC/C^{CDC20} lacking the APC4, APC5 and APC15 subunits (5G04.PDB) (Zhang et al., 2016), APC2's WHB domain that is invisible in APC/C^{CDC20} (4YII.PDB) (Brown et al., 2015), two copies of a CDC20-KEN-box complex (4GGD.PDB) (Tian et al., 2012) corresponding to $CDC20_A$–KEN2 and $CDC20_M$–KEN1, human BUBR1 (3SI5.PDB) (Bolanos-Garcia et al., 2011), and a human MAD2-peptide complex (2QYF.PDB) (Yang et al., 2007). Additional peptide segments were placed based on homology to other CDC20 or CDH1 complexes with D-boxes, KEN-boxes, or ABBA-motifs (He et al., 2013; Tian et al., 2012), or to BUBR1 homologs (Bolanos-Garcia et al., 2009; Chao et al., 2012; D'Arcy et al., 2010; Krenn et al., 2012). Because the APC4 lever-like helices/bundle are rotated relative to the propeller, APC4's propeller, helical and bundle domains were fit separately with the composite APC4 having a correlation to the map (4.8 Å) of 87% (Figure S5E). Residue changes, modeling into the peptide-like density for the pre-KEN region and CDC20 linker, deletion of residues in regions not visible in the map, joining the segments of APC4, and rigid body refinement were performed using COOT (Emsley and Cowtan, 2004).
(B) Model of human MCC core superimposed on the crystal structure of *S.pombe* MCC (4AEZ.PDB) (Chao et al., 2012).
(C) Density observed at the interface of BUBR1 and MAD2 was attributed to the linker between the KILR motif and β-propeller domain of $CDC20_M$.

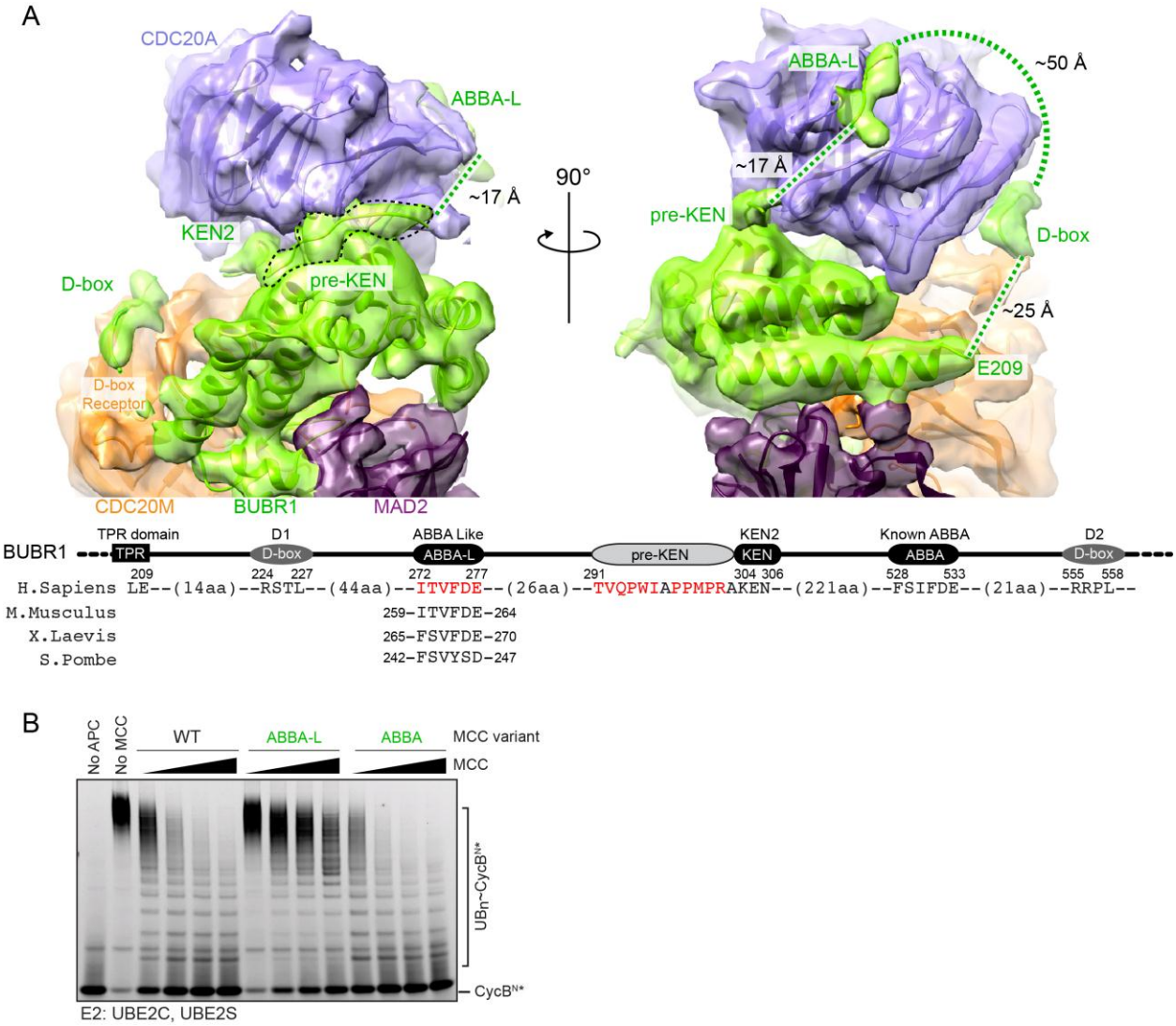

Figure S3. MCC elements mediating interactions with $CDC20_A$, as visualized in cryo EM reconstruction for APC/C^{CDC20}Δ15-MCC in CLOSED configuration. Related to Figure 3.

(A) EM reconstruction of APC/C^{CDC20}–MCC in CLOSED configuration showed density upstream of the pre-KEN/KEN peptide-like sequence resembling CDC20 interactions with an ABBA/Phe-box motif (Di Fiore et al., 2015; Diaz-Martinez et al., 2015; He et al., 2013; Lu et al., 2014). Due to sequence similarity of this region (ITVFDE) to an ABBA motif (e.g FSIFDE), we refer to this as ABBA-like (ABBA-L). The corresponding sequences of ABBA-L from *M.musculus*, *X. laevis* and *S. pombe* are shown below that of *H. sapiens* BUBR1.
(B) Assay testing effects of mutating BUBR1's ABBA-L and ABBA motif on MCC inhibition of substrate ubiquitination by APC/C^{CDC20}. Reaction products for APC/C^{CDC20}/UBE2C/UBE2S-dependent ubiquitination of the substrate $CycB^{N}$*, while titrating increasing concentrations of WT or BUBR1 ABBA-L (Ala substitutions for residues 272-277) or ABBA (Ala substitutions for residues 528-534) mutant MCC, were detected by fluorescent scan after SDS-PAGE.

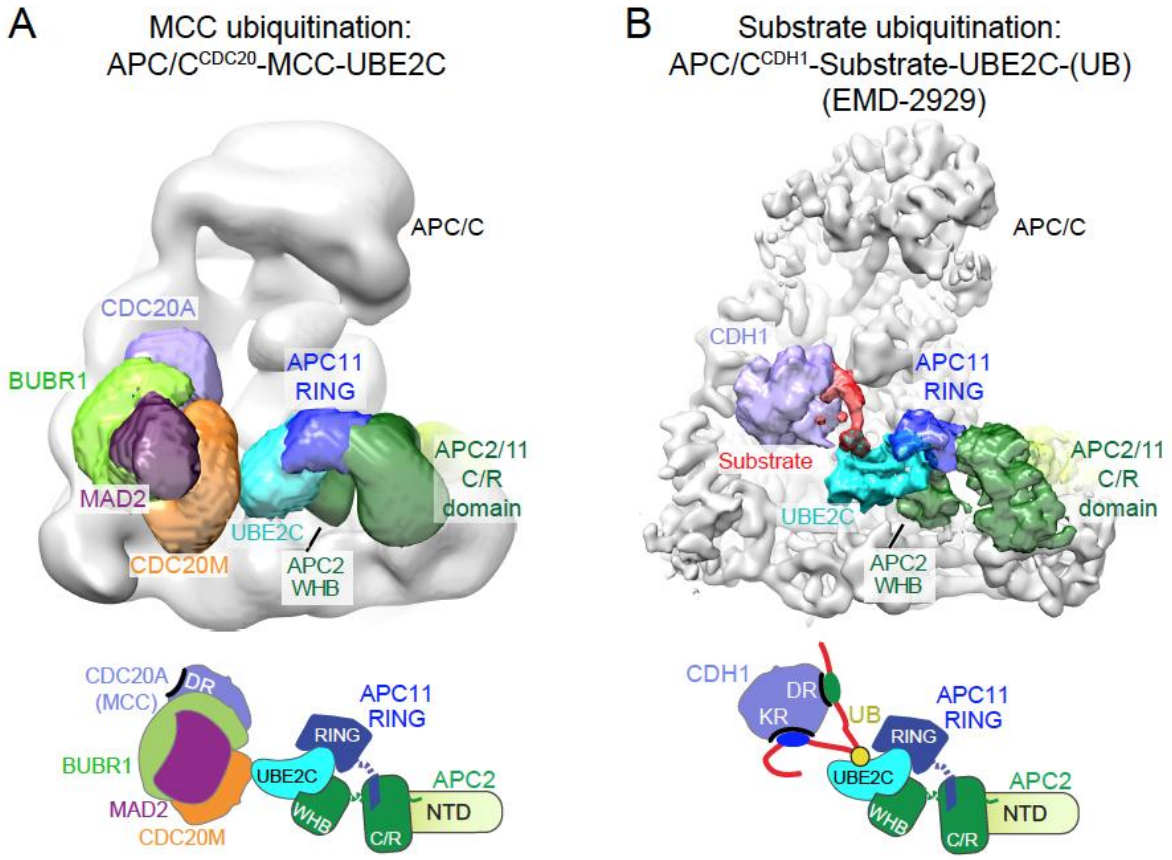

Figure S4. APC/C uses a common cullin-RING (APC2-APC11) structural mechanism to recruit, activate, and place UBE2C for ubiquitination of MCC's $CDC20_M$ or of a substrate. Related to Figure 4.
(A) Negative stain EM reconstruction of APC/C^{CDC20}–MCC–UBE2C with UBE2C's active site cross-linked to a preferred site of ubiquitination of $CDC20_M$ (residue 490, normally a Lys but here a Cys) prepared as in Figure 4D.
(B) Cryo EM reconstruction of an APC/C^{CDH1}–Substrate–UBE2C–UB complex, representing the architecture for substrate ubiquitination with UBE2C's active site cross-linked to a preferred site of ubiquitination from a peptide corresponding to the substrate Hsl1 (Brown et al., 2015). As described previously for the structural studies of substrate ubiquitination, the "donor" UB is not visible in the EM maps presumably due to conformational flexibility (Brown et al., 2015).

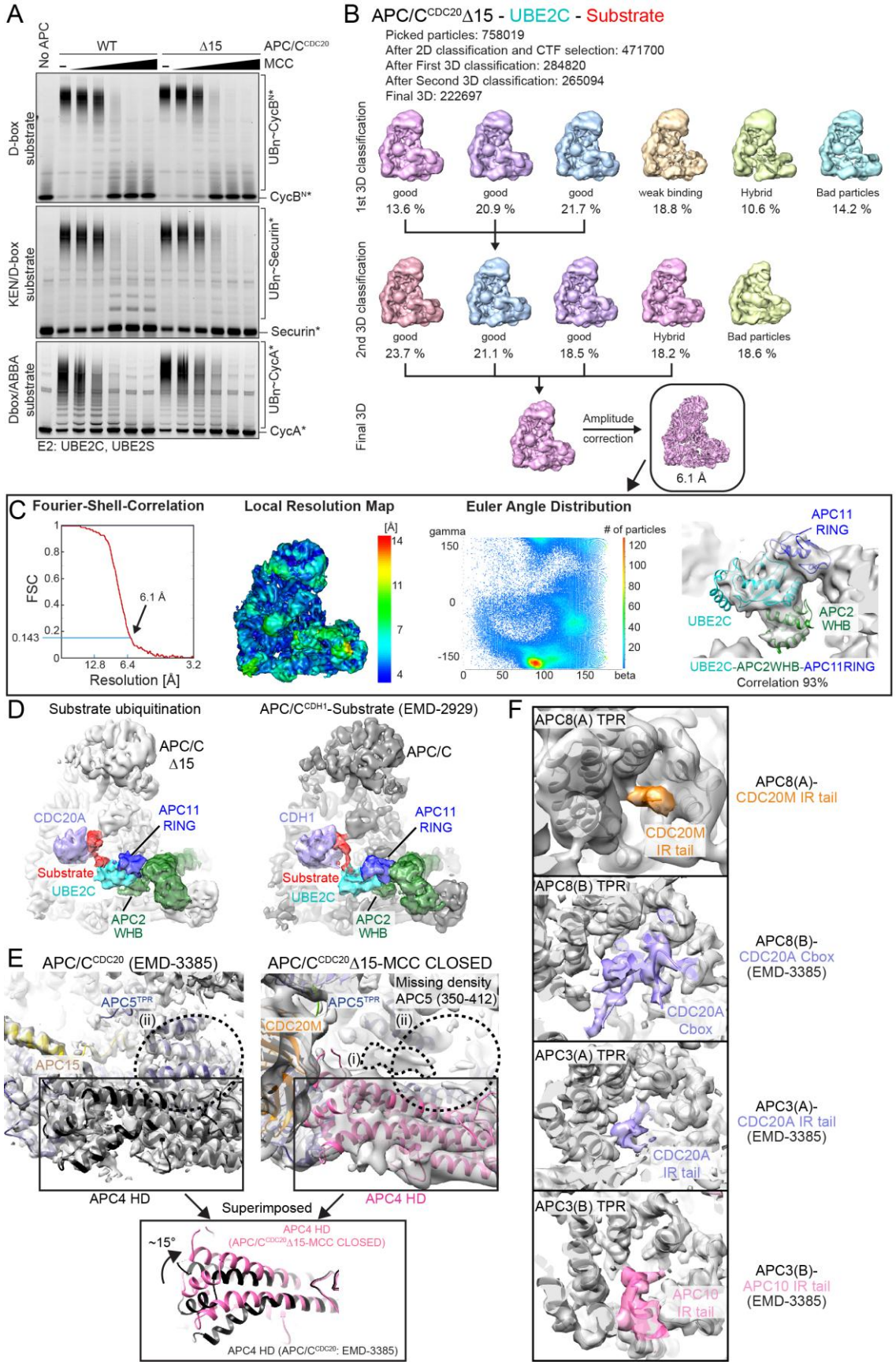
A
No APC
WT
Δ15
APC/C^CDC20
MCC
D-box substrate
KEN/D-box substrate
Dbox/ABBA substrate
UBn~CycB^N*
CycB^N*
UBn~Securin*
Securin*
UBn~CycA*
CycA*
E2: UBE2C, UBE2S
B
APC/C^CDC20Δ15 - UBE2C - Substrate
Picked particles: 758019
After 2D classification and CTF selection: 471700
After First 3D classification: 284820
After Second 3D classification: 265094
Final 3D: 222697
1st 3D classification
good 13.6 %
good 20.9 %
good 21.7 %
weak binding 18.8 %
Hybrid 10.6 %
Bad particles 14.2 %
2nd 3D classification
good 23.7 %
good 21.1 %
good 18.5 %
Hybrid 18.2 %
Bad particles 18.6 %
Final 3D
Amplitude correction
6.1 Å
C
Fourier-Shell-Correlation
FSC
0.143
6.1 Å
Resolution [Å]
Local Resolution Map
[Å]
Euler Angle Distribution
gamma
# of particles
beta
APC11 RING
UBE2C
APC2 WHB
UBE2C-APC2WHB-APC11RING
Correlation 93%
D
Substrate ubiquitination
APC/C^CDH1-Substrate (EMD-2929)
APC/C Δ15
CDC20A
APC11 RING
Substrate
UBE2C
APC2 WHB
APC/C
CDH1
E
APC/C^CDC20 (EMD-3385)
APC/C^CDC20Δ15-MCC CLOSED
APC5^TPR
(ii)
APC15
Missing density APC5 (350-412)
CDC20M
(i)
APC4 HD
Superimposed
~15°
APC4 HD (APC/C^CDC20Δ15-MCC CLOSED)
APC4 HD (APC/C^CDC20: EMD-3385)
F
APC8(A) TPR
CDC20M IR tail
APC8(A)-CDC20M IR tail
APC8(B) TPR
CDC20A Cbox
APC8(B)-CDC20A Cbox (EMD-3385)
APC3(A) TPR
CDC20A IR tail
APC3(A)-CDC20A IR tail (EMD-3385)
APC3(B) TPR
APC10 IR tail
APC3(B)-APC10 IR tail (EMD-3385)

Figure S5. Biochemical and structural characterization of APC/C^{CDC20}ΔAPC15. Related to Figure 5, 6.
(A) Assays monitoring MCC inhibition of ubiquitination of fluorescent substrates (CycB^{N}*, Securin*, or CycA*) by WT APC/C^{CDC20} or the mutant lacking the subunit APC15.
(B) The 3D reconstruction representing an APC/C^{CDC20}Δ15-UBE2C-UB-Substrate complex was determined in similar fashion to that described in Figure S2 for APC/C^{CDC20}Δ15-MCC in the CLOSED configuration. 758,019 particles were initially imaged and processed through particle sorting of 2D images and two rounds of 3D classification. Ultimately 222,697 particle images were used in the final refinement resulting in a 6.1 Å 3D structure.
(C) The Euler angle distribution, gold-standard Fourier-shell-correlation curve and local resolution map associated with these data are displayed. A model for APC/C^{CDC20}Δ15-UBE2C-substrate was generated in Chimera (Pettersen et al., 2004), by fitting the high resolution structures of APC/C^{CDC20} (5G04.PDB, without the APC15 subunit or APC11 RING domain; APC2 WHB domain is already absent in the coordinates) (Zhang et al., 2016), the crystal structure of a complex between APC2's WHB domain bound to UBE2C (4YII.PDB) and with APC11's RING domain docked on UBE2C as for the closely-related RBX1-E2 complex (Brown et al., 2015; Brown et al., 2014; Scott et al., 2014). As described previously for the EM reconstruction representing APC/C^{CDH1}-UBE2C-catalyzed substrate ubiquitination, the "donor" UB is not visible in the EM maps (Brown et al., 2015).
(D) Side-by-side comparison of EM reconstructions representing substrate ubiquitination with UBE2C. To the left is data for an APC/C^{CDC20}Δ15-UBE2C-substrate(-UB) complex, which superimposes well with the prior EM map of an APC/C^{CDH1}-UBE2C-substrate(-UB) complex (Brown et al., 2015). The "donor UB" is not visible in either map, potentially due to mobility (Pruneda et al., 2012), or due to our crosslinking method. This comparison shows that the removal of APC15 has little global effect on the potential for a coactivator-bound APC/C to recruit, activate, and place UBE2C.
(E) The EM density and models associated with the interface of APC4, APC5, and APC15 are shown for an APC/C^{CDC20}-substrate complex on the left (EMD-3385; 5G04.PDB) (Zhang et al., 2016), and APC/C^{CDC20}Δ15–MCC on the right. In comparison to WT complexes, EM maps for complexes lacking APC15 also lack clear density for three TPR helices from APC5 (residues 350-412), and instead there is evidence for a helix repacking in the TPR groove. The APC4 helical bundle domain, and the adjacent APC5 N-terminal domain contact an APC15 helix in WT APC/C, are relatively rotated in APC/C^{CDC20}Δ15–MCC in the CLOSED configuration (below). It seems that deleting APC15 influences the conformational malleability in this region in a manner that favors formation of the CLOSED configuration for APC/C^{CDC20}–MCC but does not obviously impact formation of the catalytic architecture for substrate ubiquitination.
(F) Comparison of IR tail/Cbox binding pockets in APC8/APC3. From top to bottom, APC8(A)-CDC20$_{M}$ IR tail as in Figure 6D, APC8(B)-CDC20$_{A}$ Cbox (EMD-3385), APC3(A)-CDC20$_{A}$ IR tail (EMD-3385), APC3(B)-APC10 IR tail (EMD-3385) (Zhang et al., 2016).

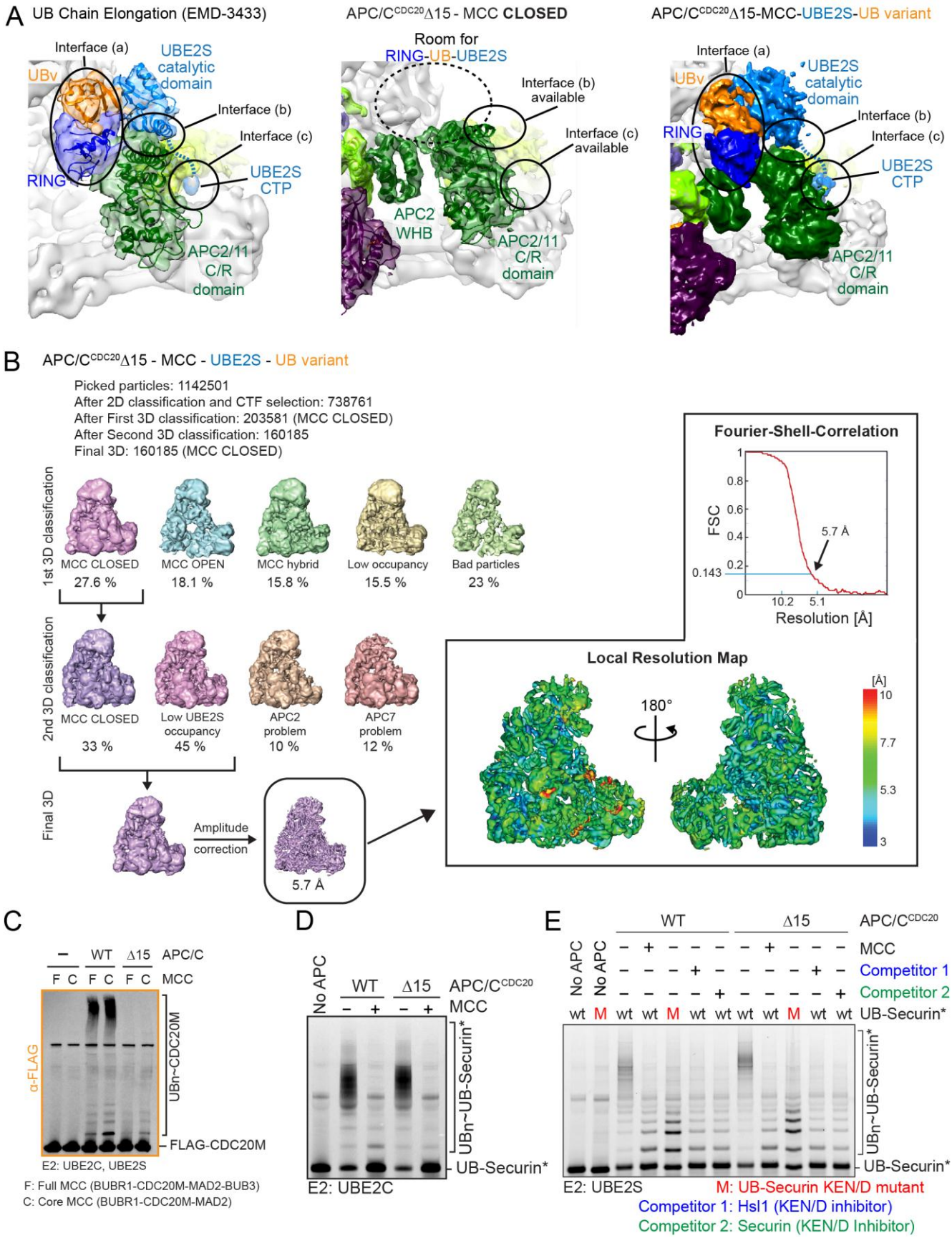
A
UB Chain Elongation (EMD-3433)
Interface (a)
UBE2S catalytic domain
UBv
Interface (b)
Interface (c)
RING
UBE2S CTP
APC2/11 C/R domain
APC/C^CDC20Δ15 - MCC CLOSED
Room for RING-UB-UBE2S
Interface (b) available
Interface (c) available
APC2 WHB
APC2/11 C/R domain
APC/C^CDC20Δ15-MCC-UBE2S-UB variant
Interface (a)
UBE2S catalytic domain
UBv
RING
Interface (b)
Interface (c)
UBE2S CTP
APC2/11 C/R domain
B
APC/C^CDC20Δ15 - MCC - UBE2S - UB variant
Picked particles: 1142501
After 2D classification and CTF selection: 738761
After First 3D classification: 203581 (MCC CLOSED)
After Second 3D classification: 160185
Final 3D: 160185 (MCC CLOSED)
1st 3D classification
MCC CLOSED 27.6 %
MCC OPEN 18.1 %
MCC hybrid 15.8 %
Low occupancy 15.5 %
Bad particles 23 %
2nd 3D classification
MCC CLOSED 33 %
Low UBE2S occupancy 45 %
APC2 problem 10 %
APC7 problem 12 %
Final 3D
Amplitude correction
5.7 Å
Fourier-Shell-Correlation
FSC
0.143
5.7 Å
Resolution [Å]
Local Resolution Map
180°
[Å]
10
7.7
5.3
3
C
– WT Δ15 APC/C
F C F C F C MCC
α-FLAG
UBn~CDC20M
FLAG-CDC20M
E2: UBE2C, UBE2S
F: Full MCC (BUBR1-CDC20M-MAD2-BUB3)
C: Core MCC (BUBR1-CDC20M-MAD2)
D
No APC
WT Δ15 APC/C^CDC20
– + – + MCC
UBn~UB-Securin*
UB-Securin*
E2: UBE2C
E
WT Δ15 APC/C^CDC20
No APC
No APC
MCC
Competitor 1
Competitor 2
wt M wt wt M wt wt wt wt M wt wt UB-Securin*
UBn~UB-Securin*
UB-Securin*
E2: UBE2S
M: UB-Securin KEN/D mutant
Competitor 1: Hsl1 (KEN/D inhibitor)
Competitor 2: Securin (KEN/D Inhibitor)

Figure S6. Structural and functional analysis of APC/C^{CDC20}–MCC activation of UBE2S-catalyzed UB chain synthesis in the presence or absence of APC15. Related to Figure 7.

(A) Side-by-side comparison of the published cryo EM reconstruction representing UBE2S poised for UB chain elongation on a UBv-fused substrate (Brown et al., 2016), of APC/C^{CDC20}Δ15-MCCcore, and of a complex between APC/C^{CDC20}Δ15-MCCcore and UBE2S with its active site cross-linked to the acceptor site (residue 11) on the UBv. The UBv (orange) is a mutant version of UB with enhanced affinity for the acceptor UB binding site on APC11's RING domain (dark blue) (Brown et al., 2016). UBE2S is shown in light blue, positioned by the previously-defined contacts to APC2 and APC4 (Brown et al., 2016). Key elements (APC11 RING's UB-binding site, APC2–APC11 C/R domain, and APC2/APC4 groove) required for UB chain synthesis by UBE2S are available in the presence of MCC.

(B) Determination of cryo EM reconstruction representing APC/C^{CDC20}Δ15-MCC, bound to UBE2S simultaneously cross-linked to a UB variant (UBv) and a donor UB mimic. This complex represents UB chain elongation by MCC-bound APC/C^{CDC20} and UBE2S. An initial 1,142,501 particles were picked of which 64.7% were kept after 2D classification and sorting. From the 1st 3D classification, 27.6% of the particles were classified with APC/C^{CDC20}Δ15-MCC in the CLOSED conformation. These particles were divided into four classes with 78% being intact APC/C-MCC particles but 45% having low occupancy of UBE2S, potentially due to a lack of anchoring without a substrate fused to the UBv (Brown et al., 2016), or due to a lack of specific enrichment for the crosslinked UBE2S-UBv-UB moiety during purification. The final three-dimensional reconstruction was computed with particles having both high and low UBE2S occupancy to a final resolution of 5.7 Å. The Gold-standard Fourier-Shell-Correlation was used to determine the resolution and we show opposing views of local resolution maps to demonstrate the resolution range.

(C) Experiment comparing full MCC and MCCcore for high molecular weight ubiquitin conjugate formation on $CDC20_M$ in the presence of UBE2S and UBE2C, with WT APC/C^{CDC20} or the mutant lacking APC15. There is no obvious impact of the presence or absence of BUB3 on $CDC20_M$ ubiquitination in this assay.

(D) Fluorescent scan of reactions testing if MCC inhibits ubiquitination of UB-Securin* by UBE2C and either WT APC/C^{CDC20} or the mutant lacking APC15. MCC concentration was 250 nM.

(E) UB chain elongation on fluorescent UB-Securin* by WT or Δ15 APC/C^{CDC20} and UBE2S. Inhibition by MCC was compared with WT activity toward KEN/D-box mutant UB-Securin* or inhibiting KEN/D-box-binding with excess cold Hsl1 or Securin.

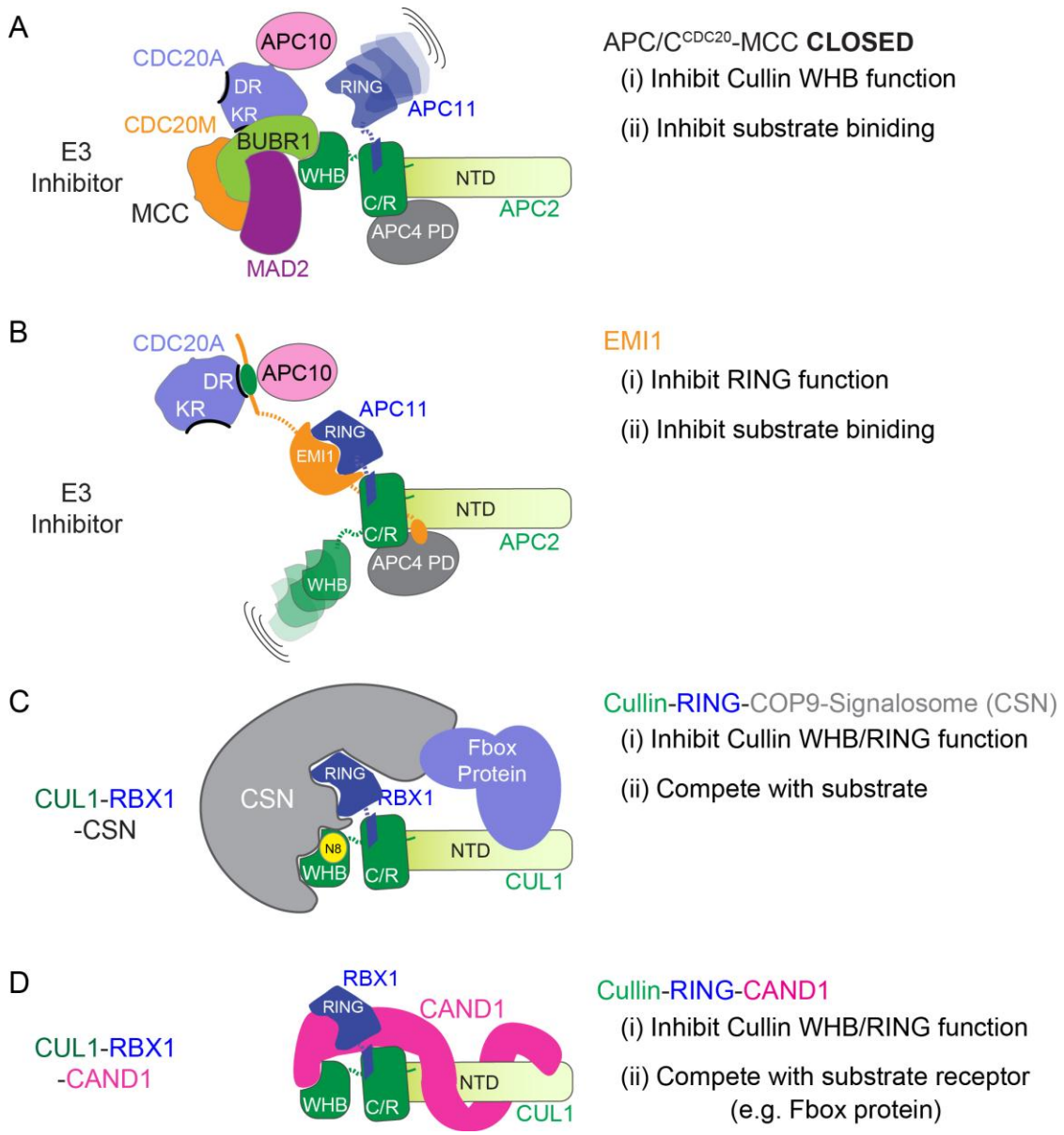

Figure S7. Multifunctional modulators of Cullin-RING Ligases. Related to Figure 7.

(A) MCC acts solely as an inhibitor when bound to APC/C^{CDC20} in the CLOSED configuration. This inhibits substrate binding to CDC20$_A$ via its key elements: D, KEN, ABBA-L, pre-KEN. In addition, MCC blocks UBE2C binding surface on APC2 WHB domain, inhibiting ubiquitination. However, conformational modulation, whereby APC/C^{CDC20}-MCC adopts an OPEN conformation allows CDC20$_M$ ubiquitination.
(B) During interphase, APC/C associates with a distinct coactivator CDH1, but binding to substrates, UBE2C and UBE2S are all blocked by EMI1 (Chang et al., 2015; Frye et al., 2013; Miller et al., 2006; Reimann et al., 2001; Wang and Kirschner, 2013).
(C, D) Classic "inhibitors" of cullin-RING ligases also depend on multisite binding and serve multiple functions. Perhaps the best-studied examples are the COP9 Signalosome (CSN, C) and CAND1 (D), which function in an intricate cycle involving dynamic protein-protein interactions and post-translational modifications to actually activate E3 ligase assembly, while likewise inhibiting post-translational modification of the cullin required for activity as indicated in the figure (Cavadini et al., 2016; Emberley et al., 2012; Enchev et al., 2012; Fischer et al., 2011; Goldenberg et al., 2004; Liu et al., 2002; Mosadeghi et al., 2016; Pierce et al., 2013; Siergiejuk et al., 2009; Wu et al., 2013; Zemla et al., 2013; Zheng et al., 2002).

Table S1. Statistics of EM reconstructions. Related to Figure 1-7.

Sample	EM Technique	Image frames	Particles in final 3D reconstruction	Resolution (Å)	Pixel size (Å)	EMDB / PDB Code	Figures
1) APC/C^{CDC20}-MCC **CLOSED**	CRYO	No	53143 (12.3%)	9	1.57	4023	1B, 1C, 2C
2) APC/C^{CDC20} – MCC **OPEN**	CRYO	No	57076 (13.2%)	10	1.57	4024	1B, 1C, 2D
3) APC/C^{CDC20}Δ15-MCC **CLOSED**	CRYO	Yes (17)	268851 (24.6%)	4.8	1.27	4021/ 5KHU	3B, 3C, 5D, 6B, 6D, S2A, S2C, S3A, S5E, S5F, S6A
4) APC/C^{CDC20}Δ15-MCC **OPEN**	CRYO	Yes (17)	86398 (7.9%)	9	1.27	4022	5E, 5F, S2A
5) APC/C^{CDC20}Δ15 - UBE2C-UB-substrate	CRYO	No	222697 (29.4%)	6.1	1.57	4025/ 5KHR	5C, S5B, S5C, S5D
6) APC/C^{CDC20}Δ15 – MCC - UBE2S-UBvariant-Ub	CRYO	Yes (17)	160,185 (14.0%)	5.7	1.57	4026	7D, S6A, S6B
7) APC/C^{CDC20}– MCC-UBE2C	NEGATIVE STAIN	No	(21.7%)	17	2.32	4027	4E, S4A
8) APC/C^{CDC20}Δ15– MCC - UBE2C	NEGATIVE STAIN	No	25472 (13%)	18	2.32	4028	6A
9) APC/C^{CDC20}– MCC **CLOSED**	NEGATIVE STAIN	No	9590 (5.4%)	20	2.5	NA	1D, 1E
10) APC/C^{CDC20}Δ15– MCC **OPEN**	NEGATIVE STAIN	No	15274 (8.6%)	20	2.5	NA	1D, 1E
11) APC/C^{CDC20}-MCCcore **CLOSED**	NEGATIVE STAIN	No	10548 (11.0%)	18	2.5	NA	1F, 1G
12) APC/C^{CDC20}-MCCcore **OPEN**	NEGATIVE STAIN	No	8726 (9.1%)	18	2.5	NA	1F, 1G

Table S2. APC/C^{CDC20}-MCC list of samples prepared for EM. Related to Figure 1, 5, 7.

		APC/C Affinity tags	CDC20	MCC	Purification Scheme	CLOSED/ OPEN Ratio
Cryo EM	***Fig. 1B***	APC4-Strep	WT	WT	1	ND
	Fig. 5D	APC4-Strep	WT	pE-core	2	ND
	Fig. 5C	Strep-APC2 /GST-APC16	WT	-	3	ND
	Fig. 7D	APC4-Strep	WT	pE-core	2	ND
Negative Stain EM (Fig. 5G, Fig. S1D)	***1 + APC15***	APC4-Strep	WT	WT	4	1.14
	1 - APC15					No OPEN
	2 + APC15 *	APC4-Strep	WT	pE	4	1.49
	2 - APC15 *					3.24
	3 + APC15 *	APC4-Strep	WT	pE-core	2	1.00
	3 - APC15 *					2.30
	4 + APC15 *	Strep-APC2 /GST-APC16	WT	pE	3	0.55
	4 - APC15 *					1.66
	5 + APC15 *	Strep-APC2 /GST-APC16	WT	pE-core	3	1.00
	5 - APC15 *					2.96
	6 + APC15	APC4-Strep	6A	WT	4	0.84
	6 - APC15					No OPEN
	7 + APC15	APC4-Strep	6A	pE-core	4	0.48
	7 - APC15					4.13

* CLOSED/OPEN ratio used in Figure S1D

Variants

6A: S41A, T55A, T59A, T69A, T70A, T106A in CDC20
pE: S41E, T70E, S92E, T106E, S368E in CDC20
and S367E, S435E, S543E, T600E, S665E, S670E, S720E, S1043E in BUBR1
core: No BUB3

Purification Scheme

1) APC/C-MCC coexpression > Strep Affinity > FLAG Affinity
2) APC/C-CDC20 colysis > Strep Affinity > Mix MCC > FLAG Affinity
3) APC/C-CDC20 colysis > Strep Affinity > GST Affinity > Mix MCC > FLAG Affinity
4) APC/C-CDC20 colysis > Strep Affinity > Anion Exchange > Size Exclusion > Mix MCC > FLAG Affinity

Table S3. Summary of APC2-APC11 catalytic core position (UP/DOWN) in APC/C-MCC sample. Related to Figure 5.

APC/C^{CDC20}-MCC prep	# of Samples	# of classes OPEN	OPEN/ UP	OPEN/ DOWN
WT	7	16	16	0
Δ15	13	14	1	13

Supplemental Movie S1. Dynamics between CLOSED and OPEN configurations of APC/C^{CDC20}-MCC shown by morphing cryo EM maps. See also Figure 1.

Supplemental Movie S2. Dynamics between CLOSED and OPEN configurations of APC/C^{CDC20}-MCC shown by morphing MCC model on superimposed cryo EM maps. See also Figure 1.

Supplemental Movie S3. Dynamics of the OPEN configuration of APC/C^{CDC20}-MCC shown by morphing negative stain EM maps. See also Figure 1.

Supplemental Experimental Procedures

Protein Purification.

For ubiquitination assays, human APC/C and its variants, UBA1, UBE2C and its variants, UBE2S, and donor UB were purified as described (Brown et al., 2015; Brown et al., 2014; Yamaguchi et al., 2015). APC/C in this study has 68 Ser and Thr residues that are sites of mitotic phosphorylation mutated to glutamates (Qiao et al., 2016). Because the APC/C contains two protomers of APC3, APC6, APC7, APC8, and CDC26/APC12, there are 100 total glutamate substitutions within the complex (Qiao et al., 2016). Unlabeled substrates Securin and Hsl1 (768-842) and labeled substrates, which were single cysteine versions of CyclinB^{N}* (residues 1-95), Securin* and acceptor UB*, were purified and fluorescently labeled, as denoted by an askterisk (*), with fluorescein-5 maleimide as described previously (Brown et al., 2015; Brown et al., 2014; Yamaguchi et al., 2015). CyclinA2 was expressed as a GST-TEV-GGGG-Strep- fusion protein in BL21 (DE3) Codon Plus (RIL) *Escherichia coli* cells and purified by GST affinity chromatography followed by affinity tag cleavage by TEV protease. The resultant GGGG-Strep-CyclinA2 was further purified by size exclusion chromatography (SEC). CyclinA2 was then fluorescently labeled by Sortase A (Dorr et al., 2014; Mao et al., 2004; Theile et al., 2013)mediated fusion of a fluorescein-5 maleimide containing Leu-Pro-Glu-Thr-Gly-Gly peptide and then further purified by Streptactin affinity chromatography and SEC. 3xMyc-HIS$_6$-CDC20 (Myc-CDC20$_A$) was expressed in High Five insect cells (Thermo Fisher Scientific), and purified by nickel affinity, cation exchange, and SEC. Specifically, cells were resuspended in buffer (20 mM HEPES, pH 7.0, 100 mM $(NH_4)_2SO4$, 2.5% glycerol, and 2mM DTT) and supplemented with protease inhibitors, lysed by sonication, and the cell lysate clarified by centrifugation (32,500xg, 60 min). Myc-CDC20$_A$ was extracted from the lysate with HIS-Select Nickel Affinity Gel (Sigma), washed with buffer and eluted with buffer supplemented with 250 mM Imidazole. Myc-CDC20$_A$ was then captured on SP sepharose (Sigma), washed with buffer supplemented with 100 mM NaCl and eluted with a gradient to 400 mM NaCl. Finally, Myc-CDC20$_A$ is put over a Superdex200 (GE Life Sciences) in 20 mM HEPES pH 7.0, 300 mM $(NH_4)_2SO4$, 2.5% glycerol, and 2mM DTT. MCC and its variants were also expressed in High Five insect cells with an N-terminal HIS$_6$-FLAG tag on BUBR1 and purified in a similar scheme as Myc-CDC20$_A$ with the following exceptions: buffer consisted of 20 mM HEPES, pH 7.5, 200 mM NaCl, 2 mM DTT, when necessary the affinity tag was cleaved by TEV protease during overnight dialysis (20 mM HEPES, pH 7.5, 100 mM NaCl, 2 mM DTT), MCC was eluted from SP sepharose with a gradient to 500 mM NaCl, and the final buffer for SEC was 20 mM HEPES pH 7.5, 200 mM NaCl, 2 mM DTT. Alternatively, MCC was also prepared by two-step affinity purification, in like buffers, via an N-terminal HIS$_6$ tag on BUBR1 and an N-terminal GST tag on MAD2 followed by SEC. The mutants used in this study are the following: KEN-box receptor (N329A/N331A/T377A/R445A), CRY-box (C165D/R166D/Y167A), K485R/K490R, and 6A (S41A/T55A/T59A/T69A/ T70A/ T106A), ΔCbox (Δ77-83), ΔCTR (Δ491-499), ΔIR (Δ498-499) for CDC20, and S201D/T204D, L205D/L208D, S201D/T204D/L205D/L208D, R169D/D172A/Q176A/Q197A/L205D/L208D, D1 (R224A/L227A), KEN2 (K304A/E305A/N306A), pre-KEN (T291A/V292A/Q293A/P294A/W295A/I296A/P298A/P299A/ M300A/P301A/R302A), ABBA-L (I272A/T273A/V274A/F275A/D276A/E277A), ABBA (F528A/S529A/I530A/F531A/D532A/E533A) for BUBR1 (Izawa and Pines, 2015; Labit et al., 2012; Reis et al., 2006; Tian et al., 2012).

Preparation of APC/C^{CDC20}-MCC for Electron Microscopy (EM)

Recombinant APC/C^{CDC20}-MCC for use in structural studies by EM was prepared by either coexpression of APC/C ^{CDC20}-MCC or mixing of purified components. For co-expression, High Five insect cells were co-infected with three baculoviruses containing all the subunits of APC/C and MCC including a Twin-Strep-tag on the C-terminus of APC4 and a HIS$_6$-FLAG tag on the N-terminus of BUBR1. Cell pellets were resuspended in lysis buffer (50 mM HEPES, pH 8.0, 250 mM NaCl, 5% glycerol, 2 mM DTT, 2 mM Benzamidine (Sigma), and 5 units/ml benzonase (Sigma), 10 µg/ml Leupeptin (Sigma), 20 µg/ml Aprotnin (Sigma), 1 EDTA-free protease inhibitor tablet per 50 mL (Roche)), lysed by sonication, and clarified by centrifugation at 32,500 xg. Purification of APC/C^{CDC20} or APC/C^{CDC20}-MCC from the clarified lysate was carried out by affinity purification on Strep-Tactin sepharose (IBA) and subsequent immunopurification on anti-DYKDDDDK G1 Affinity Resin (GenScript) following resin manufacturer protocols with a base buffer consisting of 50 mM HEPES, pH 8.0, 200 mM NaCl, 2.5% glycerol, 0.5 mM TCEP and 2 mM Benzamidine. 2.5 mM Desthiobiotin and 150 µg/ml FLAG peptide was added to the base buffer for elution from the Strep-Tactin sepharose and anti-DYKDDDDK G1 Affinity Resin, respectively.

For samples where purified components were combined, APC/C^{CDC20} was first prepared by co-lysing cells expressing APC/C or CDC20 followed by either a single affinity purification step via a C-terminal Twin-Strep-tag on APC4, dual affinity purification steps via N-terminal Twin-Strep-tag and GST tag on APC2 and APC16, respectively, or by the affinity purification, anion exchange, and SEC. The Strep affinity step was performed as

described above. For the GST affinity step, the Streptactin eluate was loaded directly on to equilibrated GS4B resin (GE Life Sciences), washed with base buffer and eluted with 20 mM reduced glutathione. The anion exchange and SEC steps were performed as described previously (Brown et al., 2015; Brown et al., 2014; Yamaguchi et al., 2015). Purified APC/C^{CDC20} was incubated with a substoichiometric amount of purified MCC or MCC-UBE2C, HRV14 3C protease to remove the affinity tags from APC/C, and anti-DYKDDDDK G1 Affinity Resin for one hour before washing the resin with base buffer and eluting with FLAG peptide. 110 ug of purified APC/C ^{CDC20}-MCC was loaded onto a GraFix gradient (Kastner et al., 2008), consisting of 10%–40% glycerol, 0.025%-0.1% gluteraldehyde, 50 mM HEPES pH 8.0, 200 mM NaCl, 2 mM MgCl2. Centrifugation was performed at 34,000 rpm in a SW55TI rotor (Beckman) for 15 hr at 4°C. The peak protein fraction of the gradient as determined by BioRad protein assay was used for EM studies.

Preparing complex representing APC/C^{CDC20}Δ15 with UBE2C active site targeting a substrate.

Our approach for trapping APC/C complexes with UBE2C active site targeting a substrate has been described (Brown et al., 2015; Brown et al., 2016). Briefly, UBE2C and target, with or without a UB representing a donor, are crosslinked based on our finding that combining several poor affinity interactors enables avidly capturing catalytically-relevant binding sites within APC/C. Toward this end, model substrates and targets are first identified biochemically, prior to designing peptide or protein targets. Here, the "substrate" was a peptide derived from the high affinity binding substrate yeast Hsl1, with the residue corresponding to the preferred ubiquitination site (normally Lys788) modified for crosslinking to a version of UBE2C harboring a single Cys at the active site. The cross-linked UBE2C-Substrate complex was prepared as previously described, with a FLAG-tagged donor UB mimic harboring a C-terminal Cys (Brown et al., 2015). Purified APC/C^{CDC20} was incubated with a substoichiometric amount of purified 3-way crosslinked UBE2C-Substrate-UB complex, with treated HRV14 3C protease to remove the affinity tags from APC/C, and purified by FLAG affinity chromatography. The APC/C^{CDC20}-UBE2C-Substrate complex was polished through GraFix for EM analysis as stated above.

Preparing APC/C^{CDC20}-MCC-UBE2C and APC/C^{CDC20}Δ15-MCC-UBE2C complexes.

The same protocol was used to generate complexes for WT APC/C^{CDC20} and the mutant expressed without APC15. The crosslinking strategy to generate a complex with UBE2C's active site affixed to a preferred target (normally Lys490 but here a Cys) was largely similar to that previously described (Brown et al., 2015; Kamadurai et al., 2013). First, a peptide (CDC20^{C}) was synthesized corresponding to 19-residues of CDC20's C-terminus, with the K490C substitution, and four N-terminal glycines (acetyl-GGGGKASAA"C"SSLIHQGIR-NH_2). A 2-way cross-linked complex was then formed between our single Cys version of UBE2C (C102A)-Strep and CDC20^{C} using the scheme illustrated in Figure 4D. Briefly, the proteins were treated with 10 mM DTT for 30 min before they were desalted into 50 mM HEPES 7.0, 400 mM NaCl. UBE2C was modified by addition 10 molar excess of BMOE (Thermo Fisher Scientific) for 15 min on ice. After removing unreacted BMOE by desalting, CDC20^{C}-UBE2C was prepared by reacting the CDC20^{C} with the UBE2C-BMOE at a 5:1 ratio for 1 hour at room temperature. The reaction was quenched with 10 mM β-mercaptoethanol and further purified by SEC. CDC20^{C}-UBE2C was then fused to the C-terminus of CDC20 in MCC by Sortase A mediated protein ligation as described (Dorr et al., 2014; Mao et al., 2004; Theile et al., 2013). In brief, MCC harboring CDC20 with a C-terminal LPETGG sequence at residue 476 (MCC^{LPETGG}), was expressed and purified as above. Then, 5 μM MCC^{LPETGG} and 20 μM CDC20^{C}-UBE2C were mixed at 4°C overnight with buffer containing 50 mM Tris pH 7.5, 150 mM NaCl, 10 mM $CaCl_2$ and 2 μM Sortase A. The resultant MCC-UBE2C complex was further purified by SEC and Strep affinity chromatography. Finally, MCC-UBE2C complex was mixed with purified APC/C^{CDC20} and APC/C^{CDC20}-MCC-UBE2C complex was immunoprecipitated based on an N-terminal FLAG tag on BUBR1, and polished through GraFix for EM analysis as described above for APC/C^{CDC20}-MCC alone.

Preparing APC/C^{CDC20}-MCC-UBE2S-UBv-UB complex.

Normally, UBE2S extends UB chains by catalyzing linkage of UB's Gly76 (donor) to Lys11 on an acceptor UB. Although UBE2S preferentially extends chains from UB-linked to D-/KEN- substrates at least in part due to their higher affinity and greater lifetime on APC/C^{CDC20}, intrinsic catalytic activity relies on specialized UBE2S recruitment to and activation by APC/C, as well as a distinct surface on APC11's RING domain reducing the K_m for the acceptor UB (Brown et al., 2014; Kelly et al., 2014). As such, APC/C^{CDC20} stimulates UBE2S-catalyzed linkage of UB to a free UB acceptor (di-UB synthesis) even in the absence of a substrate. Because structural analyses have been hampered by the extremely low affinity of an acceptor UB for APC11's RING domain, we previously used phage display to select a UB variant (UBv) with higher affinity for APC11's RING

domain, which when linked to a D-box peptide and cross-linked to the active site of UBE2S stabilized a complex representing UB chain elongation for structural studies (Brown et al., 2016).

Although MCC blocks binding to a KEN and/or D-box peptide, we considered that APC/C^{CDC20}Δ15 efficiently stimulated UBE2S-mediated di-UB synthesis in the presence of MCC (Figure 7B). To visualize this, we generated a trap with UBE2S's active site simultaneously 3-way cross-linked to residue 11 on the UBv and a Cys replacement for UB's C-terminus on a "donor" UB. Although the constructs used vary slightly, the same crosslinking strategy was used to generate cross-linked UBE2S-UBv-UB as that previously reported (Brown et al., 2016). APC/C^{CDC20}Δ15 was prepared by STREP affinity purification as described above, mixed with 2x molar excess purified MCC, incubated with HRV14 3C protease which removed affinity tags from APC4 of APC/C and then purified by SEC in 50 mM HEPES, pH 8.0, 200 mM NaCl, 2.5% glycerol, 0.5 mM TCEP. Peak fractions of the APC/CΔ15^{CDC20}-MCC complex were mixed in a 1:2 molar with UBE2S-UBv-UB and were further purified by immunoprecipitation using a FLAG tag on BUBR1 of MCC core, and by GraFix in a manner similar to that described above for APC/C^{CDC20}□□□□.

Enzyme Assays.

The qualitative APC/C-mediated ubiquitination assays were largely performed as previously described except for using 500 nM UBE2C and UBE2S, 150 nM CDC20, 90 nM fluorescently labeled (CycB^{N}*, Securin* and CycA*) plus the addition of MCC at 15, 30, 60, 120 and 250 nM (Brown et al., 2015; Yamaguchi et al., 2015). 15-250 nM of MCC was used in Figure 1A, 3E, 5B, 7B, S5A. 30-250 nM of MCC was used in Figure 3D, S3B.The ubiquitination of UB-Securin* was monitored in the presence of 250 nM MCC, 1000 nM free Hsl1 or 1000 nM free Securin. Each APC/C-mediated substrate ubiquitination experiment was subjected to SDS-PAGE and resulting gels were imaged with a Typhoon FLA 9500.

CDC20 ubiquitination assays were developed from the previously described assay using methylated UB to probe yeast Cdc20 ubiquitination (Foe et al., 2011; Foster and Morgan, 2012). 90 nM APC/C, 150 nM Myc-CDC20$_A$ and 250 nM MCC harboring FLAG-CDC20$_M$, and 90 nM CycB^{N}* when specified were incubated at 30°C with a mixture containing 100 nM E1, 500 nM UBE2C and/or UBE2S, 5 mM Mg/ATP and 150 μM UB or methylated UB. The MCC concentration was chosen based on the saturation of inhibition in substrate ubiquitination experiments. Reactions were quenched with SDS containing buffer at 2.5 min and 15 min for UB and methylated UB, respectively. The products of ubiquitination were analyzed by western blot. Specifically, Myc-CDC20$_A$ and Myc-CDC20$_A$~UBn products were detected by α-cMyc antibodies (sc-789, Santa Cruz) and α-rabbit IgG conjugated with DyLight 488 (Thermo Fisher Scientific) and FLAG-CDC20$_M$ and FLAG-CDC20$_M$~UBn products were detected by α-FLAG antibodies (F1804, SIGMA) and α-mouse IgG conjugated with Alexa Fluor 633 (Thermo Fisher Scientific). Western blot membranes were imaged with a Typhoon FLA 9500.

Western blot to confirm the absence of APC15 in recombinant APC/CΔ15.

The absence of APC15 in purified APC/CΔ15 was validated by western blot detecting APC3, APC10 and APC15 with α-APC3 (sc-9972, Santa Cruz), α-APC10 (sc-20989, Santa Cruz) and α-APC15 (sc-398488, Santa Cruz) antibodies, respectively.

Negative stain electron microscopy

Purified complexes were adsorbed to a thin film of carbon and then transferred to an electron microscopy grid covered with a perforated carbon film. The bound APC/C particles were stained with 2% (w/v) uranyl formate, blotted and air-dried for ~1 min at room temperature. Images were recorded at a magnification of 120,560× or 157,550× on a 4k × 4k CCD camera (TVIPS GmbH) using two-fold pixel binning (2.32 Å or 1.78 Å per pixel) in a Philips CM200 FEG electron microscope (Philips/FEI) operated at an acceleration voltage of 160 kV. At least 1000 images were recorded per dataset, particles were picked as described (Frye et al., 2013), and 3D classification was performed using RELION 1.3 (Scheres, 2012).

Cryo-electron microscopy

For cryo-EM, the GraFix fraction containing the desired complex was subjected to a buffer exchange procedure using Zeba spin columns (Pierce) to remove the glycerol prior to EM grid preparation. APC/C particles were allowed to adsorb on a thin film of carbon for 2 min, transferred onto a cryo-EM grid (Quantifoil 3.5/1, Jena) and then plunged into liquid ethane under controlled environmental conditions of 4 °C and 100% humidity in a vitrification device (Vitrobot Mark IV, FEI Company, Eindhoven). Images were recorded at low temperature on a Falcon II direct detector with a Titan Krios electron microscope (FEI, Eindhoven) equipped with an XFEG electron source and a Cs corrector (CEOS, Heidelberg) using 300 kV acceleration voltage. An electron dose of ~40 electrons

per $Å^2$, −0.7 to −3.5 μm defocus and a nominal magnification of 94,000× were used, resulting in a final calibrated pixel size of ~1.57 Å. CTF correction was performed by CTFFIND (Rohou and Grigorieff, 2015 JSB). Initial 2D sorting of images was performed based on CTF parameters. Only images showing isotropic Thon rings better than 6 Å were used for further processing. Additional image sorting was performed by applying several rounds of multivariate statistics, first without alignment and subsequently after image alignment to remove ice contaminations and bad particle images. The remaining good particle images were used for further processing. 3D classification in RELION 1.3 was used to obtain the particles revealing the highest MCC factor occupancy (Scheres, 2012). The best class was then used for the final refinement using the 'gold- standard procedure' in RELION 1.3. The final resolution was calculated by the Fourier-shell-correlation using the FSC 0.143 criterion and applying a soft mask with 7 voxel drop-off.

*Structure analysis***.**

Structural modeling is described in Figure S2A and Figure S5C.

In Figure 5G, S1D and Table S2, the ratio of APC/C^{CDC20}-MCC CLOSED over OPEN was determined by dividing the percent of particles in negative stain EM structural classes that adopt the CLOSED conformation by the percent of particles in structural classes that adopt OPEN conformations.

In Figure 5H and Table S3, the number of classes that represent OPEN/UP and OPEN/DOWN was determined.

Pymol and Chimera were used to generate figures of structures and EM densities (Pettersen et al., 2004; Schrodinger, 2010).

Supplemental References

Bolanos-Garcia, V.M., Kiyomitsu, T., D'Arcy, S., Chirgadze, D.Y., Grossmann, J.G., Matak-Vinkovic, D., Venkitaraman, A.R., Yanagida, M., Robinson, C.V., and Blundell, T.L. (2009). The crystal structure of the N-terminal region of BUB1 provides insight into the mechanism of BUB1 recruitment to kinetochores. Structure *17*, 105-116.

Bolanos-Garcia, V.M., Lischetti, T., Matak-Vinkovic, D., Cota, E., Simpson, P.J., Chirgadze, D.Y., Spring, D.R., Robinson, C.V., Nilsson, J., and Blundell, T.L. (2011). Structure of a Blinkin-BUBR1 complex reveals an interaction crucial for kinetochore-mitotic checkpoint regulation via an unanticipated binding Site. Structure *19*, 1691-1700.

Brown, N.G., VanderLinden, R., Watson, E.R., Qiao, R., Grace, C.R., Yamaguchi, M., Weissmann, F., Frye, J.J., Dube, P., Ei Cho, S., *et al.* (2015). RING E3 mechanism for ubiquitin ligation to a disordered substrate visualized for human anaphase-promoting complex. Proceedings of the National Academy of Sciences of the United States of America *112*, 5272-5279.

Brown, N.G., VanderLinden, R., Watson, E.R., Weissmann, F., Ordureau, A., Wu, K.P., Zhang, W., Yu, S., Mercredi, P.Y., Harrison, J.S., *et al.* (2016). Dual RING E3 Architectures Regulate Multiubiquitination and Ubiquitin Chain Elongation by APC/C. Cell *165*, 1440-1453.

Brown, N.G., Watson, E.R., Weissmann, F., Jarvis, M.A., VanderLinden, R., Grace, C.R., Frye, J.J., Qiao, R., Dube, P., Petzold, G., *et al.* (2014). Mechanism of polyubiquitination by human anaphase-promoting complex: RING repurposing for ubiquitin chain assembly. Molecular cell *56*, 246-260.

Cavadini, S., Fischer, E.S., Bunker, R.D., Potenza, A., Lingaraju, G.M., Goldie, K.N., Mohamed, W.I., Faty, M., Petzold, G., Beckwith, R.E., *et al.* (2016). Cullin-RING ubiquitin E3 ligase regulation by the COP9 signalosome. Nature *531*, 598-603.

Chao, W.C., Kulkarni, K., Zhang, Z., Kong, E.H., and Barford, D. (2012). Structure of the mitotic checkpoint complex. Nature *484*, 208-213.

D'Arcy, S., Davies, O.R., Blundell, T.L., and Bolanos-Garcia, V.M. (2010). Defining the molecular basis of BubR1 kinetochore interactions and APC/C-CDC20 inhibition. The Journal of biological chemistry *285*, 14764-14776.

Di Fiore, B., Davey, N.E., Hagting, A., Izawa, D., Mansfeld, J., Gibson, T.J., and Pines, J. (2015). The ABBA Motif Binds APC/C Activators and Is Shared by APC/C Substrates and Regulators. Developmental cell *32*, 358-372.

Diaz-Martinez, L.A., Tian, W., Li, B., Warrington, R., Jia, L., Brautigam, C.A., Luo, X., and Yu, H. (2015). The Cdc20-binding Phe box of the spindle checkpoint protein BubR1 maintains the mitotic checkpoint complex during mitosis. The Journal of biological chemistry *290*, 2431-2443.

Dorr, B.M., Ham, H.O., An, C., Chaikof, E.L., and Liu, D.R. (2014). Reprogramming the specificity of sortase enzymes. Proceedings of the National Academy of Sciences of the United States of America *111*, 13343-13348.

Emberley, E.D., Mosadeghi, R., and Deshaies, R.J. (2012). Deconjugation of Nedd8 from Cul1 is directly regulated by Skp1-F-box and substrate, and the COP9 signalosome inhibits deneddylated SCF by a noncatalytic mechanism. The Journal of biological chemistry *287*, 29679-29689.

Emsley, P., and Cowtan, K. (2004). Coot: model-building tools for molecular graphics. Acta crystallographica *60*, 2126-2132.

Enchev, R.I., Scott, D.C., da Fonseca, P.C., Schreiber, A., Monda, J.K., Schulman, B.A., Peter, M., and Morris, E.P. (2012). Structural basis for a reciprocal regulation between SCF and CSN. Cell reports *2*, 616-627.

Fischer, E.S., Scrima, A., Bohm, K., Matsumoto, S., Lingaraju, G.M., Faty, M., Yasuda, T., Cavadini, S., Wakasugi, M., Hanaoka, F., *et al.* (2011). The molecular basis of CRL4DDB2/CSA ubiquitin ligase architecture, targeting, and activation. Cell *147*, 1024-1039.

Foe, I.T., Foster, S.A., Cheung, S.K., DeLuca, S.Z., Morgan, D.O., and Toczyski, D.P. (2011). Ubiquitination of Cdc20 by the APC occurs through an intramolecular mechanism. Curr Biol *21*, 1870-1877.

Foster, S.A., and Morgan, D.O. (2012). The APC/C subunit Mnd2/Apc15 promotes Cdc20 autoubiquitination and spindle assembly checkpoint inactivation. Molecular cell *47*, 921-932.

Frye, J.J., Brown, N.G., Petzold, G., Watson, E.R., Grace, C.R., Nourse, A., Jarvis, M.A., Kriwacki, R.W., Peters, J.M., Stark, H., *et al.* (2013). Electron microscopy structure of human APC/C(CDH1)-EMI1 reveals multimodal mechanism of E3 ligase shutdown. Nature structural & molecular biology *20*, 827-835.

Goldenberg, S.J., Cascio, T.C., Shumway, S.D., Garbutt, K.C., Liu, J., Xiong, Y., and Zheng, N. (2004). Structure of the Cand1-Cul1-Roc1 complex reveals regulatory mechanisms for the assembly of the multisubunit cullin-dependent ubiquitin ligases. Cell *119*, 517-528.

He, J., Chao, W.C., Zhang, Z., Yang, J., Cronin, N., and Barford, D. (2013). Insights into degron recognition by APC/C coactivators from the structure of an Acm1-Cdh1 complex. Molecular cell *50*, 649-660.

Izawa, D., and Pines, J. (2015). The mitotic checkpoint complex binds a second CDC20 to inhibit active APC/C. Nature *517*, 631-634.

Kamadurai, H.B., Qiu, Y., Deng, A., Harrison, J.S., Macdonald, C., Actis, M., Rodgrigues, P., Miller, D.J., Souphron, J., Lewis, S.M., *et al.* (2013). Mechanism of ubiquitin ligation and lysine prioritization by a HECT E3. eLIFE *2*, e00828.

Kastner, B., Fischer, N., Golas, M.M., Sander, B., Dube, P., Boehringer, D., Hartmuth, K., Deckert, J., Hauer, F., Wolf, E., *et al.* (2008). GraFix: sample preparation for single-particle electron cryomicroscopy. Nat Methods *5*, 53-55.

Kelly, A., Wickliffe, K.E., Song, L., Fedrigo, I., and Rape, M. (2014). Ubiquitin chain elongation requires E3-dependent tracking of the emerging conjugate. Molecular cell *56*, 232-245.

Krenn, V., Wehenkel, A., Li, X., Santaguida, S., and Musacchio, A. (2012). Structural analysis reveals features of the spindle checkpoint kinase Bub1-kinetochore subunit Knl1 interaction. The Journal of cell biology *196*, 451-467.

Labit, H., Fujimitsu, K., Bayin, N.S., Takaki, T., Gannon, J., and Yamano, H. (2012). Dephosphorylation of Cdc20 is required for its C-box-dependent activation of the APC/C. The EMBO journal *31*, 3351-3362.

Liu, J., Furukawa, M., Matsumoto, T., and Xiong, Y. (2002). NEDD8 modification of CUL1 dissociates p120(CAND1), an inhibitor of CUL1-SKP1 binding and SCF ligases. Molecular cell *10*, 1511-1518.

Lu, D., Hsiao, J.Y., Davey, N.E., Van Voorhis, V.A., Foster, S.A., Tang, C., and Morgan, D.O. (2014). Multiple mechanisms determine the order of APC/C substrate degradation in mitosis. The Journal of cell biology *207*, 23-39.

Mao, H., Hart, S.A., Schink, A., and Pollok, B.A. (2004). Sortase-mediated protein ligation: a new method for protein engineering. Journal of the American Chemical Society *126*, 2670-2671.

Mosadeghi, R., Reichermeier, K.M., Winkler, M., Schreiber, A., Reitsma, J.M., Zhang, Y., Stengel, F., Cao, J., Kim, M., Sweredoski, M.J., *et al.* (2016). Structural and kinetic analysis of the COP9-Signalosome activation and the cullin-RING ubiquitin ligase deneddylation cycle. Elife *5*.

Pettersen, E.F., Goddard, T.D., Huang, C.C., Couch, G.S., Greenblatt, D.M., Meng, E.C., and Ferrin, T.E. (2004). UCSF Chimera--a visualization system for exploratory research and analysis. J Comput Chem *25*, 1605-1612.

Pierce, N.W., Lee, J.E., Liu, X., Sweredoski, M.J., Graham, R.L., Larimore, E.A., Rome, M., Zheng, N., Clurman, B.E., Hess, S., *et al.* (2013). Cand1 promotes assembly of new SCF complexes through dynamic exchange of F box proteins. Cell *153*, 206-215.

Pruneda, J.N., Littlefield, P.J., Soss, S.E., Nordquist, K.A., Chazin, W.J., Brzovic, P.S., and Klevit, R.E. (2012). Structure of an E3:E2 approximately Ub Complex Reveals an Allosteric Mechanism Shared among RING/U-box Ligases. Molecular cell *47*, 933-942.

Qiao, R., Weissmann, F., Yamaguchi, M., Brown, N.G., VanderLinden, R., Imre, R., Jarvis, M.A., Brunner, M.R., Davidson, I.F., Litos, G., et al. (2016). Mechanism of APC/C^{CDC20} activation by mitotic phosphorylation. Proceedings of the National Academy of Sciences of the United States of America 113, E2570-2578.

Reis, A., Levasseur, M., Chang, H.Y., Elliott, D.J., and Jones, K.T. (2006). The CRY box: a second APCcdh1-dependent degron in mammalian cdc20. EMBO reports *7*, 1040-1045.

Scheres, S.H. (2012). RELION: implementation of a Bayesian approach to cryo-EM structure determination. Journal of structural biology *180*, 519-530.

Schrodinger, LLC (2010). The PyMOL Molecular Graphics System, Version 1.3r1.

Scott, D.C., Sviderskiy, V.O., Monda, J.K., Lydeard, J.R., Cho, S.E., Harper, J.W., and Schulman, B.A. (2014). Structure of a RING E3 Trapped in Action Reveals Ligation Mechanism for the Ubiquitin-like Protein NEDD8. Cell *157*, 1671-1684.

Siergiejuk, E., Scott, D.C., Schulman, B.A., Hofmann, K., Kurz, T., and Peter, M. (2009). Cullin neddylation and substrate-adaptors counteract SCF inhibition by the CAND1-like protein Lag2 in Saccharomyces cerevisiae. The EMBO journal *28*, 3845-3856.

Theile, C.S., Witte, M.D., Blom, A.E., Kundrat, L., Ploegh, H.L., and Guimaraes, C.P. (2013). Site-specific N-terminal labeling of proteins using sortase-mediated reactions. Nat Protoc *8*, 1800-1807.

Tian, W., Li, B., Warrington, R., Tomchick, D.R., Yu, H., and Luo, X. (2012). Structural analysis of human Cdc20 supports multisite degron recognition by APC/C. Proceedings of the National Academy of Sciences of the United States of America *109*, 18419-18424.

Wu, S., Zhu, W., Nhan, T., Toth, J.I., Petroski, M.D., and Wolf, D.A. (2013). CAND1 controls in vivo dynamics of the cullin 1-RING ubiquitin ligase repertoire. Nature communications *4*, 1642.

Yamaguchi, M., Yu, S., Qiao, R., Weissmann, F., Miller, D.J., VanderLinden, R., Brown, N.G., Frye, J.J., Peters, J.M., and Schulman, B.A. (2015). Structure of an APC3-APC16 complex: insights into assembly of the anaphase-promoting complex/cyclosome. Journal of molecular biology *427*, 1748-1764.

Yang, M., Li, B., Tomchick, D.R., Machius, M., Rizo, J., Yu, H., and Luo, X. (2007). p31comet blocks Mad2 activation through structural mimicry. Cell *131*, 744-755.

Zemla, A., Thomas, Y., Kedziora, S., Knebel, A., Wood, N.T., Rabut, G., and Kurz, T. (2013). CSN- and CAND1-dependent remodelling of the budding yeast SCF complex. Nature communications *4*, 1641.

Zhang, S., Chang, L., Alfieri, C., Zhang, Z., Yang, J., Maslen, S., Skehel, M., and Barford, D. (2016). Molecular mechanism of APC/C activation by mitotic phosphorylation. Nature *533*, 260-264.

Zheng, J., Yang, X., Harrell, J.M., Ryzhikov, S., Shim, E.H., Lykke-Andersen, K., Wei, N., Sun, H., Kobayashi, R., and Zhang, H. (2002). CAND1 binds to unneddylated CUL1 and regulates the formation of SCF ubiquitin E3 ligase complex. Molecular cell *10*, 1519-1526.